COMMUNICATION

Reversible Switching of Water-Droplet Mobility on a Superhydrophobic Surface Based on a Phase Transition of a Side-Chain Liquid-Crystal Polymer

By *Chao Li, Renwei Guo, Xi Jiang, Shuxin Hu, Lin Li, Xinyu Cao,* Huai Yang,* Yanlin Song, Yongmei Ma,* and *Lei Jiang**

Superhydrophobic surfaces with different dynamic wettabilities, such as water repellent or water adhesive, have attracted increasing interest recently.[1–8] The lotus leaf, with ultrahigh water contact angle (CA) and low sliding angle (SA), is widely known as a model superhydrophobic surface because of its self-cleaning property. Although superhydrophobic surfaces with high SA cannot be self-cleaning, they have many other potential applications, such as in the field of microfluidic control systems.[9–15] Superhydrophobic surfaces that can "pin" liquid droplets have been demonstrated for no-loss microdroplet transfer or trance-liquid reactors.[16–22] It is known that superhydrophobicity is effective for obtaining a small liquid interfacial contact area (ICA), at least for water-based liquids, which significantly reduces the mass loss in microdroplet transfer.[23] To construct more dense and complicated microfluidic devices, the integration of superhydrophobicity and reversible switching of water mobility would be desirable.

If a certain liquid is preferred, it would be better to optimize the substrate rather than modifying the liquid. A change of either the substrate's chemistry or its morphology can affect the liquid droplet mobility.[24–30] However, tuning the mobility of pure water droplets on superhydrophobic surfaces has so far been demonstrated only on different samples.[31,32] It still remains a great challenge to reversibly control water droplet mobility on the same surface, which requires the precise coordination of surface chemistry response and surface roughness.

[*] Prof. X. Y. Cao, Prof. L. Jiang, C. Li, X. Jiang, Dr. S. X. Hu, Prof. L. Li, Prof. Y. L. Song, Prof. Y. M. Ma
Beijing National Laboratory for Molecular Sciences
Center of Molecular Sciences
Institute of Chemistry
Chinese Academy of Sciences
Beijing 100190 (P.R. China)
E-mail: xinyucao@iccas.ac.cn; jianglei@iccas.ac.cn
C. Li
National Center for Nanoscience and Technology
Beijing 100190 (P.R. China)
Prof. H. Yang, R. W. Guo
Department of Materials Physics and Chemistry
School of Materials Science and Engineering
University of Science and Technology Beijing
Beijing 100083 (P. R. China)
E-mail: yanghuai@mater.ustb.edu.cn

DOI: 10.1002/adma.200900903

Here, we report on a versatile strategy that can reversibly control the mobility of spherical microdroplets of water on the same surface from rollable (SA $\leq 90^\circ$) to pinned (water droplet does not move at any tilt angle, even when the substrate is turned upside down) by temperature. Unlike previous reports on CA switchable surfaces,[33,34] this study is about water mobility switching, and furthermore, the static CAs before and after switching are all in the superhydrophobic range. The superhydrophobic surface with switchable water mobility is prepared by simply spin-coating a side-chain liquid crystal polymer (SCLCP), PDMS-4OCB, on an optimized rough silicon wafer. The molecular structure of PDMS-4OCB is illustrated in Scheme 1. It consists of hydrophobic methyl groups and relatively hydrophilic butyloxy biphenylcarbonitrile groups both attached to the polysiloxane main chain. PDMS-4OCB is a liquid crystal SmA phase at room temperature (23 °C), and undergoes a phase transition from SmA to isotropic at 74.6 °C[35] (see also the Supporting Information). The mobility switching of the water droplet is thought to be due to the abrupt change of molecular chain adaptability corresponding to the SCLCP phase transition and the coordination of the surface roughness.

On a flat PDMS-4OCB film, when the temperature increases from 23 °C to 75 °C (just above the phase transition point), the CA of a 3 μL water droplet changes from $92.4^\circ \pm 1.8^\circ$ to $89.3^\circ \pm 0.8^\circ$ (Fig. 1a). It is proposed that such a surface wettability change corresponds to a discontinuous change of the interfacial interaction caused by the (liquid) crystal-to-isotropic phase transition.[34,36–38] The mechanism is illustrated as Figure 1b. At the topmost surface of the as-prepared PDMS-4OCB film, the groups toward the air should mainly be the hydrophobic methyl groups.[34–38] In the SmA phase, the mobility of polymer chains is

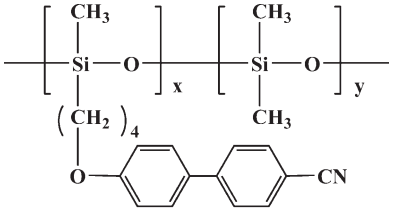

Scheme 1. The molecular formula of PDMS-4OCB.

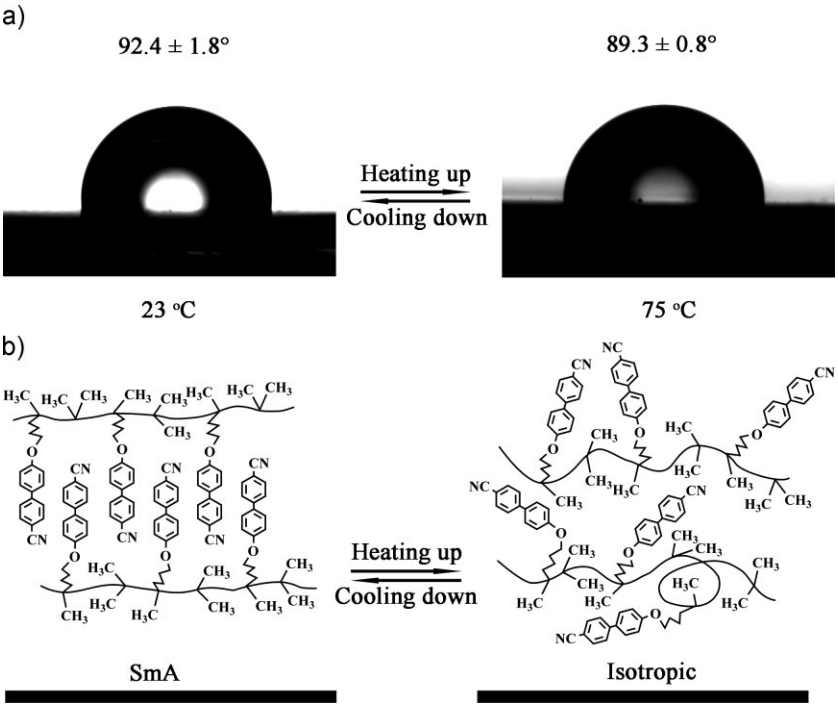

Figure 1. a) The water CA switching between 92.4° ± 1.8° at 23 °C and 89.3° ± 0.8° at 75 °C on flat PDMS-4OCB film. b) The proposed conformation rearrangement upon the phase transition corresponding to the CA switching.

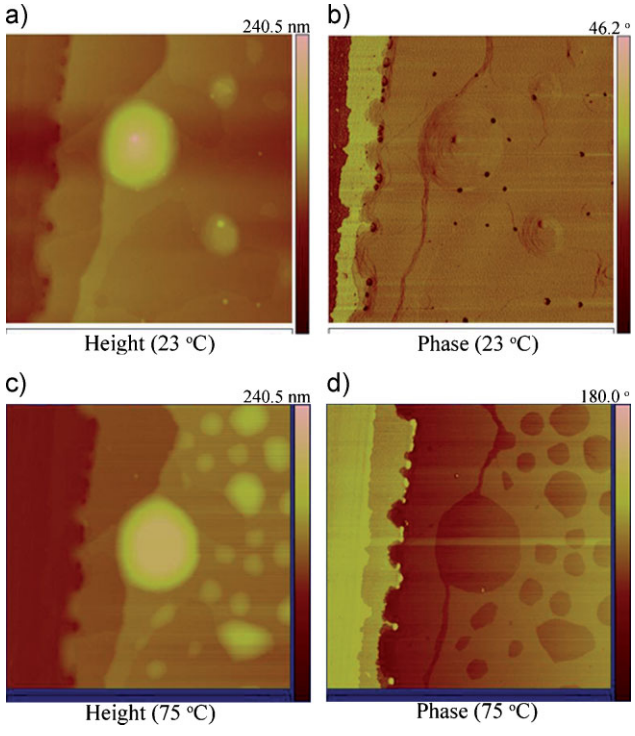

Figure 2. In situ AFM images of the a) height and b) phase of PDMS-4OCB film at 23 °C, and of the c) height and d) phase of the film at 75 °C. The scanning size of all four images is 10 μm × 10 μm.

rather low, and the molecular conformation cannot be changed by the contact of the test liquid. When the temperature increases to or above the isotropic phase transition point, the molecular chains' mobility becomes much greater. When a water droplet is deposited on the surface, the molecular chains can quickly undergo a self-adaptive process so that the more-hydrophilic groups turn towards the water to minimize the interfacial energy, thus the water CA decreases.

Besides the conformation change of the molecular chains, a change in surface roughness may also occur and contribute to the wettability change upon phase transition. However, this point has been ignored in previous research.[34–37] To measure the roughness change, in situ atomic force microscopy (AFM) observations of PDMS-4OCB film at 23 °C and 75 °C were carried out; both topographic and phase images are shown in Figure 2. The film is generally flat with micropapillae (Fig. 2a). The mean thickness of the film at 23 °C is 21.0 ± 1.7 nm. When the temperature increases to 75 °C, the film swells and the mean thickness increases to 35.4 ± 1.7 nm. Some new papillae appear at 75 °C with ca. 1 μm diameter and 20 nm height (Fig. 2c), but in terms of the average roughness analysis (box R_a), the change is not pronounced. The average roughness is 11.2 nm at 23 °C and 12.4 nm at 75 °C (see Supporting Information, Figs. S4a,b).

Furthermore, the phase images, Figure 2b,d, reveal that the film is of layered structure at 23 °C (clearly shown on the papillae, Fig. S4c, Supporting Information). The repeat layer distance (3.5 ± 0.4 nm) is identical with that of the PDMS-4OCB SmA phase.[39] The layered structure disappears at 75 °C. This indicates that the isotropic phase transition occurs, which is consistent with the differential scanning calorimetry (DSC) and polarizing optical microscopy (POM) measurements (see Supporting Information, Figs. S2 and S3).

The CA change on the flat PDMS-4OCB upon phase transition is only about 3° or even ambiguous (Fig. 1a). This is because the polarity difference of the molecular groups is limited and the roughness change is slight.

It has been reported that the synergy of micrometer- and nanometer-scale roughness may enlarge the CA and CA response range. To obtain a superhydrophobic surface, roughness has to be involved, but at the same time, the CA response range has to be confined to keep all CAs in the superhydrophobic range. Patterned surfaces with six different pattern sizes were adopted in the experiments (see the Experimental section for more details of fabrication). The rough substrates were silicon wafers with square-arrayed square posts. The post's size was constant with an area of 10 μm × 10 μm and a height of 30 μm. The typical morphology of the rough surfaces is illustrated in Figure 3a,b. Different roughness was obtained by varying the spacing between the posts. The samples were labeled S1–S6, with spacing 40, 30, 20, 15, 10, and 5 μm, respectively. CAs and SAs were then

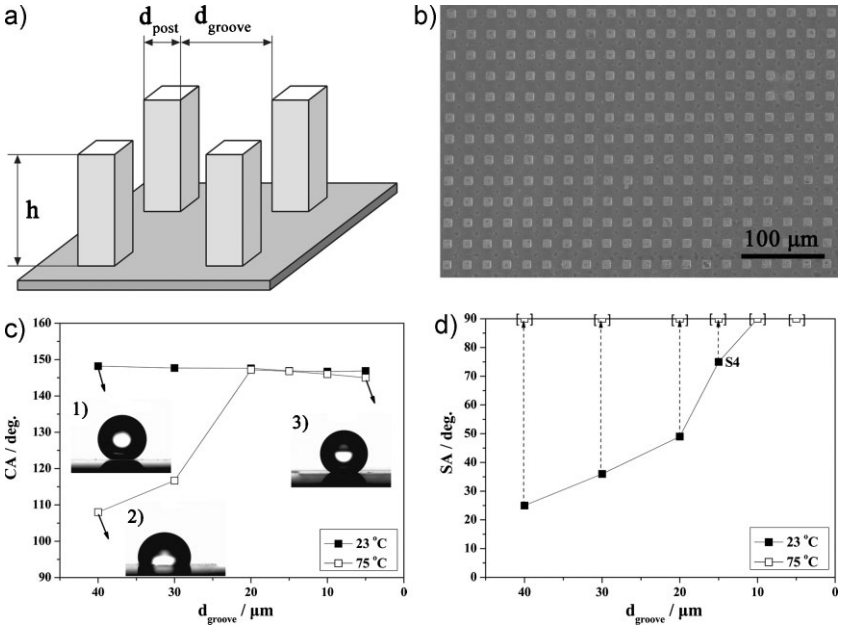

Figure 3. a) Schematic illustration of the main parameters of the square-arrayed square posts. The post width $d_{post} = 10$ μm, and the height h of posts for all substrates is 30 μm. For S1–S6, the spacings between two nearest posts d_{groove} are 40, 30, 20, 15, 10, and 5 μm, respectively. b) Typical SEM image of the PDMS-4OCB modified rough surface, which is S4. c,d) Results of measurements of CA and SA on the PDMS-4OCB modified surfaces with different d_{groove} at 23 °C (filled squares) and 75 °C (empty squares). Insets 1–3 in c) are representative profiles of a water droplet on the surfaces. In (d), the data of SA > 90° (droplet pinned) are represented by points in square brackets. The vertical arrows denote the mobility change of the water droplet on the same sample.

measured at 23 °C and 75 °C (Fig. 3c,d). The results of CA and SA response on these rough surfaces hold some surprises.

At 23 °C, the water CAs on S1–S6 are all enhanced to superhydrophobic level by the roughness (Fig. 3c). On the surfaces of S1 and S2, we obtained enhanced CA response around the phase transition temperature with the obvious collapse of CAs to less than 120° at 75 °C. However, that is what we need to avoid, so as to keep the droplet's spherical shape and small ICA. In contrast, CAs are almost unchanged in the superhydrophobic range on S3, S4, S5, and S6 at 75 °C. Further microscopic side-view observations show that the droplets on S3–S6 are in different superhydrophobic states compared to those at 23 °C, and this may lead to different droplet mobility.

Generally, there are two wettability states when a liquid droplet settles on a hydrophobic surface: the composite state and the wetted state.[23–25] It is reported that there are energy barriers that prevent the transition between the two states.[40–44] Experimentally, the wettability states can be distinguished by whether there is light between the liquid and the substrate in a microscopic side view.[9,40] The SA is mainly governed by the ICA and the three-phase contact line (TCL).[10–15] In addition, the detailed contact mode at the TCL can also make the SA different.[40–42] Even when the CAs are the same, the ICA and TCL for droplets in different wettability states can be quite different.

At 23 °C, on all these rough surfaces, the water droplets are in the superhydrophobic composite state. From S1 to S6, with the decrease of d_{groove}, the post density increases. If CA remains the same, the ICA and TCL both increase. (Actually, the CA decreases but by less than 2°, which also leads to an increase of TCL.) As a result, with decreasing d_{groove}, the SA gradually increases from 25° to more than 90° (Fig. 3d). The water droplets are rollable on S1, S2, S3, and S4, but pinned on S5 and S6.

At 75 °C, the SmA-to-isotropic phase transition occurs. For the same sample, the water–SCLCP interfacial interaction greatly increases, owing to the polymer chain self-adaptability, which consequently lowers the energy barrier of the wettability state transition. The microscopic side view observations show that the droplets are all in wetted states, and the water droplet is pinned on all the six rough surfaces (Fig. 3d). The water droplets on S1 and S2 collapse, accompanied by state transition from composite state to wetted state, and the TCL moves in both the horizontal and perpendicular directions. The dramatically increased ICA and TCL make the droplet no longer rollable. On S3, S4, S5, and S6, the superhydrophobic CAs are almost unchanged, but the droplets are in a superhydrophobic wetted state at 75 °C instead of the composite state at 23 °C. There is no evident TCL movement in the horizontal direction, but perpendicular movement of TCL occurs, with water penetrating into the microgrooves. At a certain CA, the ICA and TCL are larger in the wetted state than in the composite state for the same sample, which leads to higher SA. Consequently, the mobility of the superhydrophobic droplets substantially changes from rollable to pinned on S3 and S4. On S5 and S6 at either 23 °C or 75 °C, the water droplets are pinned, so the phase transition effect cannot be reflected in their SA change.

In addition, at 23 °C, when the water droplet is softly deposited on S3, it is in a persistent superhydrophobic composite state, but immediately after rolling, the droplet collapses. During rolling, there is a momentum. If the sum of the droplet's self-gravity and the momentum is greater than the energy barrier, the wettability state transition will occur. The spherical shape of the water droplet on S4 is quite stable. This may be explained by the effect of morphology on the energy barrier.[41,42] So the reversible switching of a superhydrophobic droplet between rollable and pinned by temperature is demonstrated further on S4 (Fig. 4). While CAs of the water droplets remain in the superhydrophobic range at both 23 °C and 75 °C, a sudden switching of droplet mobility from rollable (SA ca. 75°) to pinned occurs with the phase transition. The inset in Figure 4a shows that the droplet was still pinned on the surface even when the substrate was turned upside down. The enlarged pictures in Figure 4b show that the spherical water droplet is in the composite state at 23 °C and in the wetted state at 75 °C.

To further confirm the driving force of the switch, the temperature dependence of SA was also measured on S4 (Fig. 4c). There is almost no SA change from 23 °C to 65 °C. The sharp increase of SA only occurs near the phase transition point, which clearly indicates the interdependence of the phase transition and

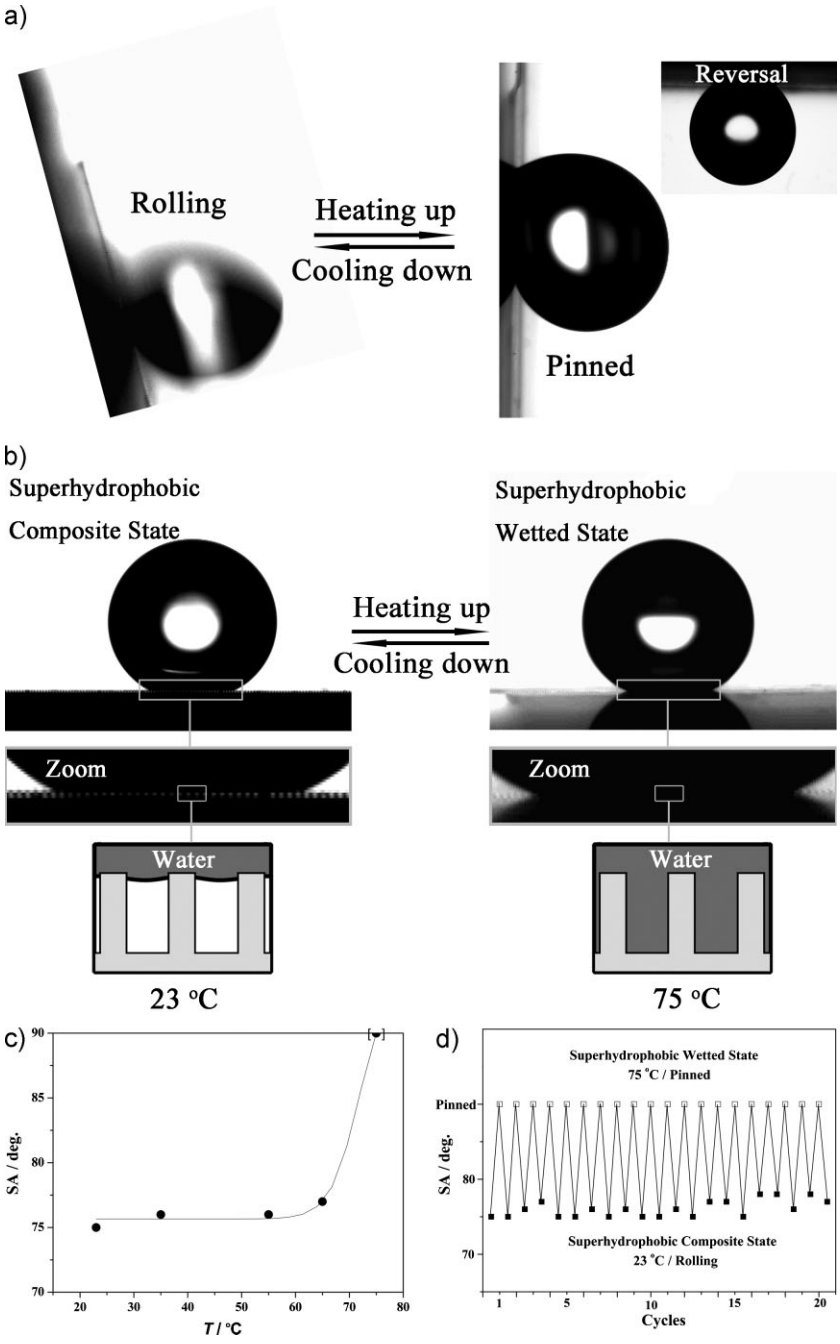

Figure 4. a) The reversible switching of the water droplet mobility from rollable to pinned corresponding to the temperature change from 23 °C (left, SA = 75° ± 3°) to 75 °C (right, the inset shows that the droplet sticks on the surface even when the substrate is turned upside down). b) At 23 °C, the water droplet is in the superhydrophobic composite state; at 75 °C, it is in the superhydrophobic wetted state. c) SAs on sample S4 at different temperatures. The curve shows an abrupt change of SA near the SmA-to-isotropic phase transition temperature of the PDMS-4OCB. d) 20 cycles measurements of water droplet mobility switching between 23 °C and 75 °C. At 23 °C, the water droplet is rollable (filled squares). At 75 °C, the water droplet is pinned (empty squares).

the switching of SA. Similar measurements were also conducted on other superhydrophobic surfaces without a phase transition (see Supporting Information, Fig. S5 and Table S3), and no obvious SA change could be observed in the temperature range of 23–75 °C (see Supporting Information, Fig. S6). The SA on S4 recovers to 75° when the substrate is cooled down to room temperature. The reversible switching of the water droplet mobility from rollable to pinned was demonstrated by at least 20 cycles of measurement (Fig. 4d) on S4 with a square area of 0.5 cm^2. Further enhancement of the film response and reversibility needs to be addressed in the future.

In conclusion, thermally reversible switching of the mobility of a 3 μL water droplet from rollable to pinned on a superhydrophobic surface has been demonstrated by spin-coating SCLCP solution on an optimized rough silicon wafer. Precise coordination of the roughness and the interfacial chemistry response that reversibly changes the ICA and TCL is essential to obtain the mobility switching. It can be easily extended to other stimuli-responsive materials and broadens the possible applications. This strategy shows promising potential applications in the construction of smart no-loss microdroplet transfer devices, microreactor devices, etc.

Experimental

Materials: PDMS-4OCB was synthesized and purified according to the literature [35,45,46]. The IR spectrum, DSC, and POM results are shown in the Supporting Information. The micrometer-post-array silicon wafers with different roughness were prepared by photolithography and an inductively coupled plasma deep-etching technique [33,34].

Preparation of SCLCP Thin Films: PDMS-4OCB solution (1 wt% in acetone) was spin-coated (Chemat spin coater KW-4A) on silicon wafers under 500 rpm (3 s) then 2000–3500 rpm (30 s). The as-prepared samples were then annealed at 75 °C for 1 h and stored in a clean box.

Characterization: *The* scanning electron microscopy (SEM) images were obtained by an environment SEM (Hitachi S-3000 at 5 kV). AFM tapping-mode images were acquired using an atomic force microscope (NanoScope IIIa MultiMode, Veeco Instruments) equipped with a high-temperature heating accessory. The set-point amplitude ratio was adjusted to be 0.7–0.9. Si tips (TESP, Digital Instruments) with a resonance frequency of approximately 300 kHz and a spring constant of about 40 N m^{-1} were used. Water CAs and SAs were measured on a contact angle system OCA20 (DataPhysics, Germany). Because the water droplet size can affect both CA and SA [9], the droplet size should be chosen so that all the results are comparable, and, furthermore, can demonstrate the droplet mobility switching while maintaining the spherical shape of the droplet. By a primary optimization of the droplet size, *3* μL was chosen in all measurements (see Supporting Information, Table S2). The average CA and SA values were obtained by measuring the same sample at least in five different positions. The experimental errors of CA and SA are less than ±2° and ±3°, respectively. The temperature was controlled by an electrical

temperature control chamber (TEC400, Germany) and samples were equilibrated at the measuring temperature for at least 5 min.

Acknowledgements

The authors thank the NSFC (Grants 50573082, 20774101), the MoST Research Program (2007CB936403, 2007AA03Z327), and the institute program CMS-CX200603. Supporting Information is available online from Wiley InterScience or from the authors.

Received: March 16, 2009
Revised: April 5, 2009
Published online: June 24, 2009

[1] L. Feng, S. Li, Y. Li, H. Li, L. Zhang, J. Zhai, Y. Song, B. Liu, L. Jiang, D. Zhu, *Adv. Mater.* **2002**, *14*, 1857.
[2] a) T. Sun, L. Feng, X. Gao, L. Jiang, *Acc. Chem. Res.* **2005**, *38*, 644. b) X. Feng, L. Jiang, *Adv. Mater.* **2006**, *18*, 3063.
[3] S. Wang, Y. Song, L. Jiang, *J. Photochem. Photobiol, C* **2007**, *8*, 18.
[4] M. Callies, D. Quéré, *Soft Matter* **2005**, *1*, 55.
[5] X. Zhang, F. Shi, J. Niu, Y. Jiang, Z. Wang, *J. Mater. Chem.* **2008**, *18*, 621.
[6] P. Roach, N. J. Shirtcliffe, M. I. Newton, *Soft Matter* **2008**, *4*, 224.
[7] L. Gao, T. J. McCarthy, *J. Am. Chem. Soc.* **2006**, *128*, 9052.
[8] Y. C. Jung, B. Bhushan, *Nanotechnology* **2006**, *17*, 4970.
[9] Z. Yoshimitsu, A. Nakajima, T. Watanabe, K. Hashimoto, *Langmuir* **2002**, *18*, 5818.
[10] X. Song, J. Zhai, Y. Wang, L. Jiang, *J. Phys. Chem. B* **2005**, *109*, 4048.
[11] M. Jin, X. Feng, L. Feng, T. Sun, J. Zhai, T. Li, L. Jiang, *Adv. Mater.* **2005**, *17*, 1977.
[12] Y. Zheng, X. Gao, L. Jiang, *Soft Matter* **2007**, *3*, 178.
[13] L. Gao, T. J. McCarthy, *Langmuir* **2006**, *22*, 2966.
[14] X. Gao, X. Yao, L. Jiang, *Langmuir* **2007**, *23*, 4886.
[15] Z. Cheng, L. Feng, L. Jiang, *Adv. Funct. Mater.* **2008**, *18*, 3219.
[16] X. Hong, X. Gao, L. Jiang, *J. Am. Chem. Soc.* **2007**, *129*, 1478.
[17] D. Huh, A. H. Tkaczyk, J. H. Bahng, Y. Chang, H. Wei, J. B. Grotberg, C. Kim, K. Kurabayashi, S. Takayama, *J. Am. Chem. Soc.* **2003**, *125*, 14678.
[18] W. Satoh, H. Hosono, H. Suzuki, *Anal. Chem.* **2005**, *77*, 6857.
[19] N. Yoshida, Y. Abe, H. Shigeta, A. Nakajima, H. Ohsaki, K. Hashimoto, T. Watanabe, *J. Am. Chem. Soc.* **2006**, *128*, 743.
[20] P. Dubois, G. Marchand, Y. Fouillet, J. Berthier, T. Douki, F. Hassine, S. Gmouh, M. Vaultier, *Anal. Chem.* **2006**, *78*, 4909.
[21] K. A. Wier, T. J. McCarthy, *Langmuir* **2006**, *22*, 2433.
[22] N. Zhao, Q. Xie, X. Kuang, S. Wang, Y. Li, X. Lu, S. Tan, J. Shen, X. Zhang, Y. Zhang, J. Xu, C. C. Han, *Adv. Funct. Mater.* **2007**, *17*, 2739.
[23] a) A. Lafuma, D. Quéré, *Nat. Mater.* **2003**, *2*, 457. b) D. Quéré, A. Lafuma, J. Bico, *Nanotechnology* **2003**, *14*, 1109.
[24] A. B. D. Cassie, S. Daxter, *Trans. Faraday Soc.* **1944**, *40*, 546.
[25] R. N. Wenzel, *Ind. Eng. Chem.* **1936**, *28*, 988.
[26] L. Jiang, R. Wang, B. Yang, T. Li, D. A. Tryk, A. Fujishima, K. Hashimoto, D. Zhu, *Pure Appl. Chem.* **2000**, *72*, 73.
[27] H. S. Lim, D. Kwak, D. Y. Lee, S. G. Lee, K. Cho, *J. Am. Chem. Soc.* **2007**, *129*, 4128.
[28] Q. Xie, G. Fan, N. Zhao, X. Guo, J. Xu, J. Dong, L. Zhang, Y. Zhang, C. C. Han, *Adv. Mater.* **2004**, *16*, 1830.
[29] Y. Ma, X. Cao, X. Feng, Y. Ma, H. Zou, *Polymer* **2007**, *48*, 7455.
[30] S. Wang, Y. Song, L. Jiang, *Nanotechnology* **2007**, *8*, 18.
[31] Y. Zhao, Q. Lu, D. Che, *J. Mater. Chem.* **2006**, *16*, 4504.
[32] Y. Yao, X. Dong, S. Hong, H. Ge, C. C. Han, *Macromol. Rapid Commun.* **2006**, *27*, 1627.
[33] T. Sun, G. Wang, L. Feng, B. Liu, Y. Ma, L. Jiang, D. Zhu, *Angew. Chem. Int. Ed.* **2004**, *43*, 357.
[34] S. Hu, X. Cao, Y. Li, P. Xie, L. Jiang, *Chem. Commun.* **2008**, 2025.
[35] H. Finkelmann, U. Kiechle, G. Rehage, *Mol. Cryst. Liq. Cryst.* **1983**, *94*, 343.
[36] G. Crevoisier, P. Fabre, J. Corpart, L. Leibler, *Science* **1999**, *285*, 1246.
[37] K. Cho, J. H. Cho, S. Yoon, C. E. Park, J. Lee, S. Han, K. Lee, J. Koo, *Macromolecules* **2003**, *36*, 2009.
[38] S. Wu, in *Polymer Interface and Adhesion*, Marcel Dekker, New York **1982**.
[39] a) P. J. Collings, *Liquid Crystals: Nature's Delicate Phase of Matter*, 2nd ed., Princeton University Press, Princeton, NJ **2002**, pp. 75–77. b) I. Dierking, *Textures of Liquid Crystals*, Wiley-VCH, Weinheim **2003**, pp. 9–12.
[40] N. A. Patankar, *Langmuir* **2004**, *20*, 7097.
[41] C. W. Extrand, *Langmuir* **2002**, *18*, 7991.
[42] C. Dorrer, J. Rühe, *Langmuir* **2006**, *22*, 7652.
[43] L. Barbieri, E. Wagner, P. Hoffmann, *Langmuir* **2007**, *23*, 1723.
[44] B. He, N. A. Patankar, J. Lee, *Langmuir* **2003**, *19*, 4999.
[45] a) H. Yang, T. Kajiyama, *Liq. Cryst.* **2000**, *27*, 721. b) H. Yang, T. Kajiyama, *Liq. Cryst.* **2002**, *29*, 1141.
[46] H. Huang, H. Yang, *Liq. Cryst.* **2007**, *34*, 949.